Research Square

Preprints are preliminary reports that have not undergone peer review.
They should not be considered conclusive, used to inform clinical practice,
or referenced by the media as validated information.

Enhanced eddy--mean-flow feedbacks increase summer North Atlantic Oscillation extremes

Quan Liu

quan.liu@mpimet.mpg.de

Max Planck Institute for Meteorology

Jürgen Bader

Universität Hamburg

Johann H. Jungclaus

Max Planck Institute for Meteorology

Daniela Matei

Max Planck Institute for Meteorology

Research Article

Keywords: North Atlantic Oscillation, extreme weather, global warming, eddy--mean-flow feedback

Posted Date: May 27th, 2026

DOI: https://doi.org/10.21203/rs.3.rs-9825988/v1

License: This work is licensed under a Creative Commons Attribution 4.0 International License.
Read Full License

Additional Declarations: The authors declare no competing interests.

Enhanced eddy–mean-flow feedbacks increase summer North Atlantic Oscillation extremes

Quan Liu[1,2*], Jürgen Bader[3], Johann H. Jungclaus[1], Daniela Matei[1]

[1*]Climate Variability Department, Max Planck Institute for Meteorology, Hamburg, Germany.

[2]International Max Planck Research School on Earth System Modelling, Hamburg, Germany.

[3]Institute of Oceanography, Center for Earth System Research and Sustainability (CEN), Universität Hamburg, Hamburg, Germany.

*Corresponding author(s). E-mail(s): quan.liu@mpimet.mpg.de;

Contributing authors: juergen.bader@uni-hamburg.de; johann.jungclaus@mpimet.mpg.de; daniela.matei@mpimet.mpg.de;

Abstract

Summer North Atlantic Oscillation (NAO) extremes can trigger contrasting severe weather conditions across northern Europe and the Mediterranean. A recent work has shown that the occurrence of both positive and negative phases of these extremes would increase under global warming, but the underlying physical mechanism is missing. Here, using daily output from large-ensemble climate change simulations, we examine how eddy forcing and eddy–mean-flow feedbacks shape the life cycle of summer NAO extremes. We show that anomalous eddy momentum forcing and Rossby wave breaking drive the occurrence of these extremes, while positive eddy–mean-flow feedback sustains their persistence.

Under global warming, this feedback strengthens through distinct pathways: enhanced barotropic feedback, associated with a northward-shifted jet, prolongs positive summer NAO extremes, while enhanced baroclinic feedback, associated with stronger high-latitude blocking, prolongs negative extremes. These results indicate that competing atmospheric responses to global warming, which represent a "tug of war" in the mean circulation, amplify opposite phases of summer NAO extremes, increasing likelihood of contrasting extreme weather across the North Atlantic–European sector.

Keywords: North Atlantic Oscillation, extreme weather, global warming, eddy–mean-flow feedback

1 Introduction

The North Atlantic Oscillation (NAO) is a mode of large-scale atmospheric variability. It exhibits strong internal variability across a wide range of timescales [1, 2], driving contrasting weather patterns between northern Europe and the Mediterranean [3]. Recently, an analysis based on large-ensemble climate change simulations and reanalysis data showed that anthropogenic warming changes both the mean state and variability of the summer NAO index: it drives a positive trend in the mean state and increases the occurrence and impacts of both positive and negative summer NAO extremes [4]. However, the physical mechanisms driving the increase in extremes remain unknown.

The persistence of summer NAO extremes is sustained by positive feedbacks. In fact, the NAO variability itself on timescales longer than synoptic scales relies on a positive feedback between eddy momentum fluxes and zonal-wind (U) anomalies [5, 6]. In this feedback, the effect of eddy momentum fluxes on U anomalies is well understood through the zonal-mean eddy momentum budget [7]. Conversely, the effect of U anomalies on eddies can be divided into two families: a baroclinic mechanism, in which U anomalies modify the collocated baroclinic instability and hence the upward

flux of wave activity into the upper troposphere [8–12]; and a barotropic mechanism, in which U anomalies directly alter meridional wave propagation by shifting Rossby-wave critical levels or turning latitudes, independent of changes in the baroclinic wave source [9, 10, 12, 13].

Therefore, the projected increase in summer NAO extremes may be due to enhanced eddy–mean-flow feedbacks that prolong the persistence of summer NAO variability. In this study, we first examine this positive feedback by tracking the eddy forcing of U anomalies throughout the life cycle of summer NAO extremes, using over 9000 positive extremes and over 8000 negative extremes extracted from daily output of the Max Planck Institute Grand Ensemble with CMIP6 forcing (MPI-GE-CMIP6) (Methods) [14]. To investigate how global warming modifies the feedback through both barotropic and baroclinic pathways, we investigate changes in the upper-level eddy sink and lower-level eddy source across different levels of warming. Our analysis shows that global warming modifies the effect of U anomalies on eddies and, in turn, the effect of eddies on U anomalies, which closes the positive feedback loop.

2 Result

2.1 Eddy forcing of U anomalies drives the occurrence of summer NAO extremes

We begin by linking the summer NAO variability to eddy forcing of the upper-level U anomalies. During positive summer NAO extremes, the upper-level subpolar jet is displaced northward (Fig. 1a), while during negative summer NAO extremes, the subpolar jet is located farther south, merging with the subtropical jet (Fig. 1b). Therefore, the summer NAO variability is associated with a meridional shift of upper-level U anomalies (Fig. 1c), consistent with its winter counterpart [15].

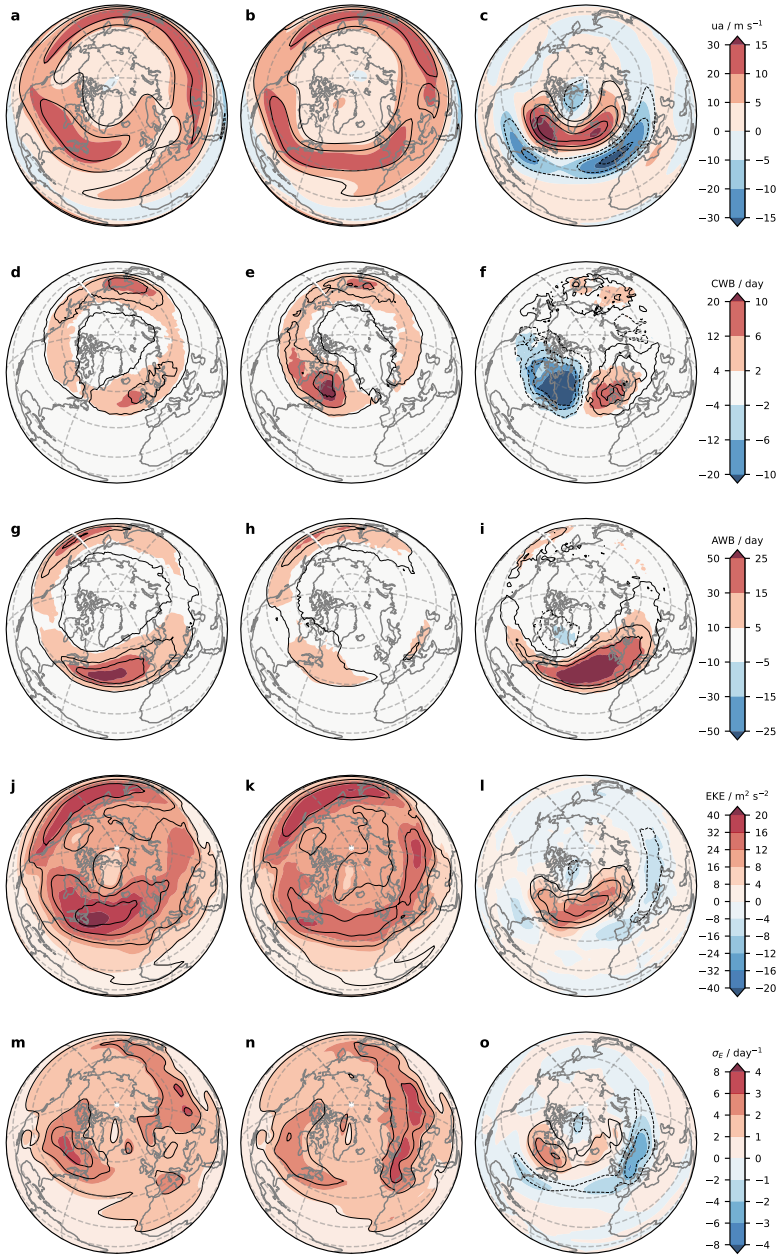

Fig. 1 The eddy forcing of U anomalies drives occurrence of summer NAO extremes. Columns show composites for positive summer NAO extremes (**a,d,g,j,m**), negative summer NAO extremes (**b,e,h,k,n**) and their difference (**c,f,i,l,o**), averaged from day −5 to day +5 relative to event onset. Rows show the 250-hPa zonal wind (**a-c**), cyclonic wave breaking (CWB; **d-f**), anticyclonic wave breaking (AWB; **g-i**), mid-tropospheric eddy kinetic energy (EKE; **j-l**) and eddy growth rate (σ_E; **m-o**). Shading shows composites for the first decade (1850s), and contours show the corresponding composites for the last decade (2090s). Contours use the same levels as the shading, with the zero contour omitted. Composites are sums for CWB and AWB, and means for the other fields. See Methods for the definitions of CWB, AWB, EKE and eddy growth rate.

This meridional shift of U anomalies across summer NAO phases is driven by eddy forcing. A framework to diagnose this eddy forcing is the Transformed Eulerian Mean (TEM) equation [7]:

$$\frac{\partial \overline{u}}{\partial t} = f_0 \overline{v}^* + \overline{v'q'} + \overline{F} \tag{1}$$

where primes denote eddy terms and overbars denote zonal means, f_0 is the Coriolis parameter, $\overline{v}^*$ is the residual mean meridional flow, and $\overline{F}$ represents frictional forcing. The potential-vorticity flux ($\overline{v'q'}$) that drives U anomalies is defined as $\overline{v'q'} = -\frac{\partial}{\partial y}\overline{u'v'} + \frac{\partial}{\partial z}\left(\frac{f_0}{N^2}\overline{v'b'}\right)$, which can be writen as the divergence of the Eliassen-Palm (EP) flux [16], $\overline{v'q'} = \nabla \cdot \mathcal{F}$, and:

$$\mathcal{F} = -\overline{u'v'}\mathbf{j} + \frac{f_0}{N^2}\overline{v'b'}\mathbf{k} \tag{2}$$

where b represents buoyancy and N is the buoyancy frequency.

The meridional component of the EP-flux (first term in the right-hand side of Eq 2) corresponds to the eddy momentum flux convergence, and it is the direct driver of the meridional shift of the jet [5]. The northward-shifted jet during positive summer NAO extremes is due to anomalous eddy momentum flux convergence at high latitudes (Fig. S1a), driven by poleward eddy momentum flux originated from anticyclonic wave breaking on the southern side of the jet (Fig. 1g). Similarly, the southward-shifted jet during negative summer NAO extremes is due to anomalous eddy momentum flux convergence at lower latitudes (Fig. S1b), driven by cyclonic wave breaking on the northern side of the jet (Fig. 1d). The eddy momentum forcing forms the basis for the barotropic component of the eddy–mean-flow feedback, which we will examine in the next section.

The irreversible decay of Rossby waves at upper levels is sustained by eddy growth in the baroclinic zone, as reflected by the upward component of the EP-flux (second term in the right-hand side of Eq 2). This indicates that the summer NAO variability would also be modulated by lower-level eddy source. Indeed, similar to the upper-level zonal-mean flow, mid-tropospheric eddy activity, measured by eddy kinetic energy, and the eddy source, estimated by the lower-level Eady growth rate (Methods), exhibit similar meridional shifts across summer NAO phases (Fig. 1j-o). This connection between summer NAO variability and baroclinic eddy growth forms the basis of the baroclinic mechanism of eddy–mean-flow feedback.

2.2 Positive feedbacks maintain the persistence of summer NAO extremes

The TEM equation (Eq. 1) provides a framework for diagnosing the eddy forcing of U anomalies, but it does not describe how U anomalies may, in turn, influence the eddies. This feedback is key to understanding the persistence of summer NAO extremes and, therefore, the mechanism underlying their increase under global warming. We examine this feedback by tracking eddy forcing throughout the life cycle of summer NAO extremes.

For positive summer NAO extremes, the anticyclonic wave breaking on the southern side of the jet that triggers their occurrence (Fig. 1i) begins to deviate from climatology about 5 days before onset (orange lines; Fig. 2a). It then remains above climatology until about 20 days after onset—much longer than synoptic timescales. This persistence is largely maintained by barotropic feedback: the northward-shifted jet displaces the critical latitude for anticyclonic wave breaking poleward, which shifts eddy momentum flux convergence poleward and reinforces the jet at higher latitudes. This barotropic feedback is evident in Fig. 3a. During the developing stage of positive summer NAO extremes (days -5 to $+5$ relative to onset; Fig. 3ai), jet latitude increases

relatively weakly with the likelihood of anticyclonic wave breaking, except for a few very low jet-latitude values that may reflect misidentification of the subtropical jet as the subpolar jet. During the decay stage (days +10 to +20; Fig. 3aii), although more events have relatively weak anticyclonic wave breaking and lower jet latitudes (orange lines; Fig. 2a), the relationship between jet latitude and wave-breaking likelihood becomes much steeper. The role of this positive barotropic feedback in maintaining the persistence of positive summer NAO extremes is evident from the standardized slope between jet latitude and anticyclonic wave-breaking likelihood, which increases with time relative to onset (solid line; Fig. 3a).

On the contrary, the persistence of negative summer NAO extremes is mainly maintained by barolinic feedback. Unlike positive extremes, the cyclonic wave breaking that triggers negative extremes remains above climatology after the peak but drops back to climatological levels within 10 days (green lines; Fig. 2b). Meanwhile, the EP-flux divergence that reinforce the jet stream at lower-latitude remains above climatology until about 20 days after onset (green lines; Fig. 2d). This discrepancy suggests that EP-flux divergence during the decay stage of negative summer NAO extremes is sustained primarily by continuous eddy growth in the mid-latitude baroclinic zone veering equatorward aloft [7], rather than by cyclonic wave breaking. This baroclinic feedback is quanlitatively captured by anomalously high mid-tropospheric eddy activity (greenlines; Fig. 2f) and lower-level Eady growth rate (greenlines; Fig. 2e, negative anomalies at higher-latitudes corresponds to positive anomalies at lower-latitudes.) at the later stage of the negative summer NAO extremes.

The mechanism underlying this baroclinic feedback during negative summer NAO extremes lies in eddy thermal forcing. The lower-level baroclinicity that gives rise to transient eddies is associated with the meridional temperature gradient. Once generated, transient eddies transport warm air poleward and cold air equatorward,

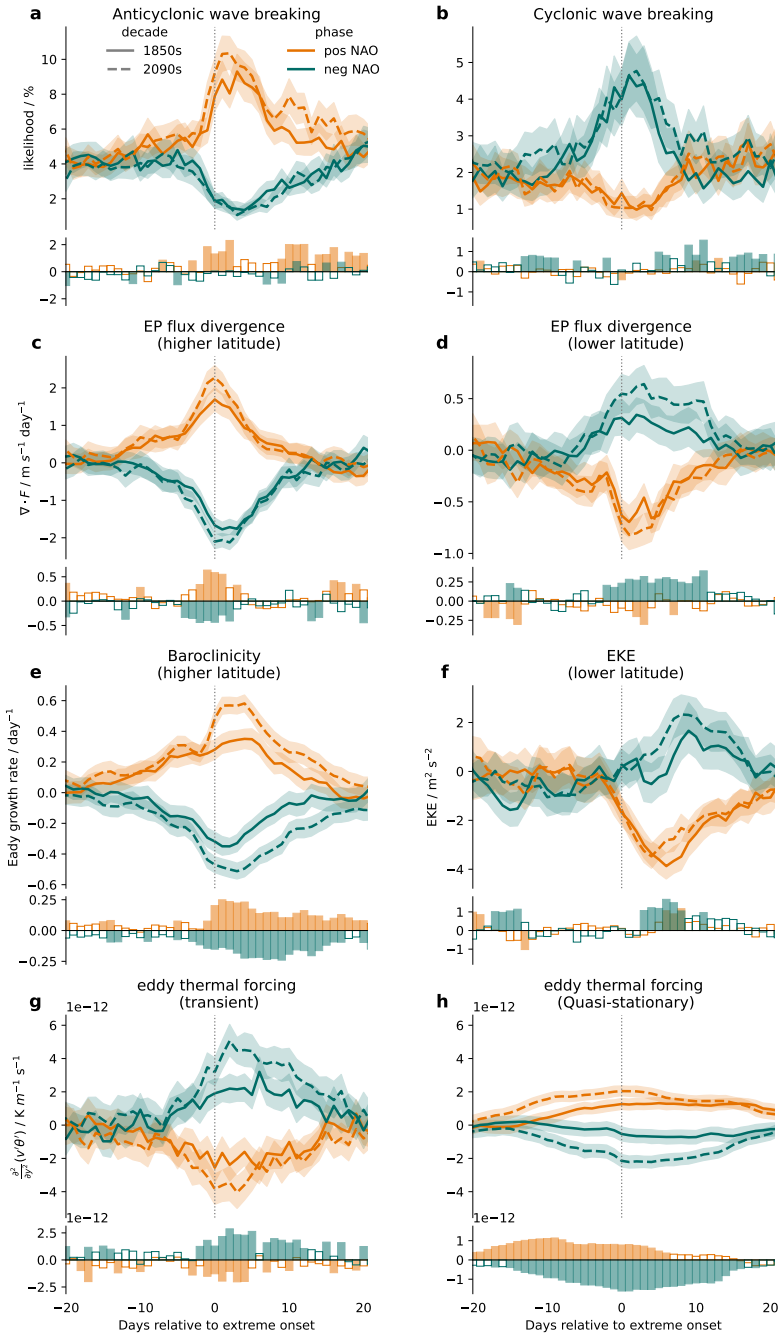

Fig. 2 Eddy–mean-flow feedbacks associated with summer NAO extremes and their changes under global warming. Panels show the evolution of key eddy-feedback terms relative to event onset. Lines denote composites for the 1850s (solid) and 2090s (dashed), and bars show their difference (2090s minus 1850s); filled bars indicate one-sided significance at the 95% confidence level. Panels show anticyclonic wave breaking (AWB; **a**), cyclonic wave breaking (CWB; **b**), upper-level EP-flux convergence over the northern flank of the jet (50–70°N; **c**) and southern flank of the jet (30–50°N; **d**), mid-tropospheric transient-eddy kinetic energy (**e**), lower-level baroclinicity (**f**), transient-eddy thermal forcing (**g**) and quasi-stationary-eddy thermal forcing (**h**). AWB is averaged over [−60°, 30°, 40°, 60°], and CWB over [−120°, −30°, 50°, 70°]. The high-latitude region is defined as [−90°, 40°, 50°, 70°], and the low-latitude region as [−90°, 40°, 30°, 50°]. Thermal forcing from both transient and quasi-stationary eddies is shown for the low-latitude region (**g**, **h**). EP-flux convergence is evaluated at 250 hPa, mid-tropospheric eddy kinetic energy at 500 hPa, and baroclinicity and thermal-forcing terms at 850 hPa.

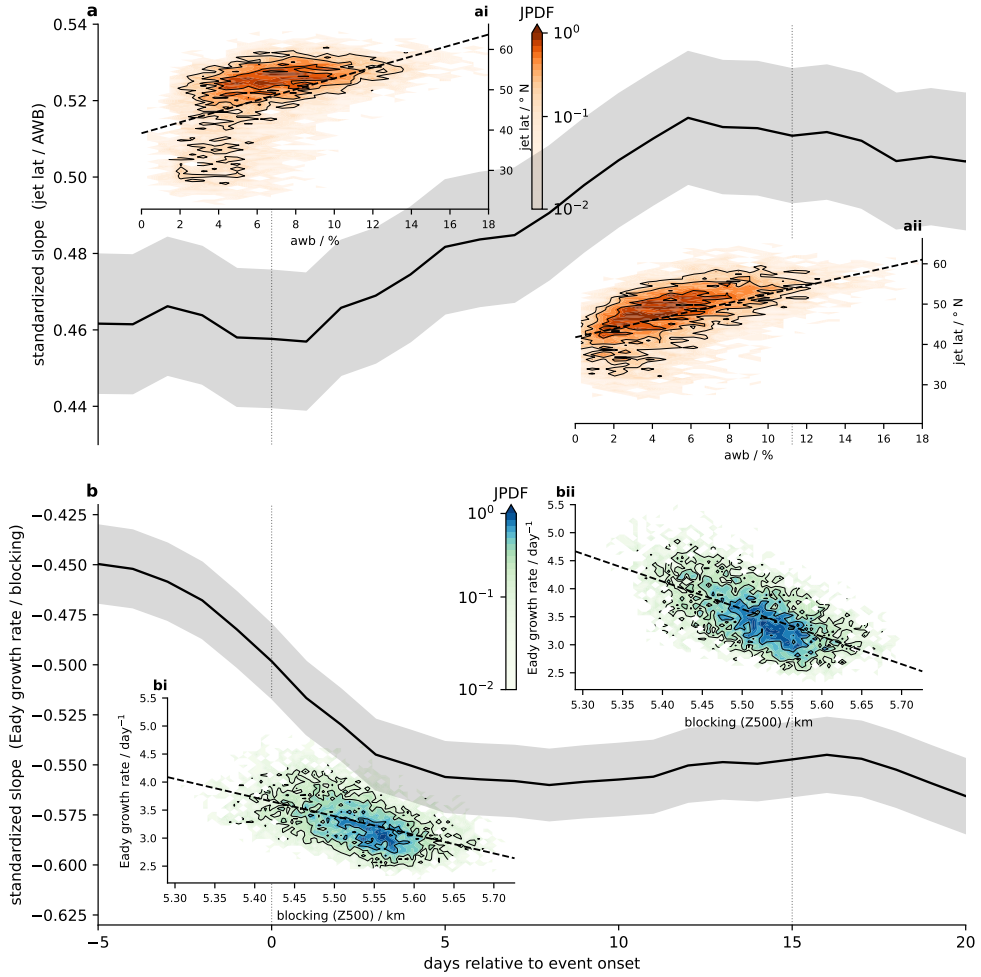

Fig. 3 Barotropic and baroclinic feedbacks maintain the persistence of positive and negative summer NAO extremes, respectively. a, Evolution of the standardized linear slope between jet latitude and anticyclonic wave-breaking likelihood during positive summer NAO extremes. Scatter plots used to estimate the slopes for days −5 to +5 and days +10 to +20 are shown in **ai** and **aii**, respectively. **b**, As in **a**, but for the relationship between Eady growth rate and the Greenland blocking index during negative summer NAO extremes; the corresponding scatter plots are shown in **bi** and **bii**. Slopes are calculated using a 10-day running window across over 9000 positive extremes and over 8000 negative extremes. Jet latitude is defined as the latitude of maximum zonal wind over the North Atlantic (90°W–40°E). Anticyclonic wave breaking is averaged over [−60°, 30°, 40°, 60°]. The Eady growth rate is averaged over [−90°, 40°, 50°, 70°]. The Greenland blocking index is defined as the 30-day running-mean 500-hPa geopotential height averaged over [−80°, −20°, 60°, 80°].

weakening the meridional temperature gradient and exerting a negative forcing on lower-level baroclinicity. This thermal forcing can be diagnosed from the meridional derivative of the zonal-mean thermodynamic equation [17, 18]:

$$\frac{\partial}{\partial t}\left(-\frac{\partial \overline{\theta}}{\partial y}\right) = \frac{\partial^2}{\partial y^2}\overline{v'\theta'} - \frac{\partial}{\partial y}\left(\Gamma\,\overline{\omega}\right) - \mathcal{R} \tag{3}$$

where θ is potential temperature; $\Gamma = -T\dfrac{\partial \ln \theta}{\partial p}$ is the static stability parameter; p denotes pressure; ω denotes vertical velocity; and $\mathcal{R}$ denotes diabatic heating. Indeed, at higher latitudes, the anomalous thermal forcing ($\frac{\partial^2}{\partial y^2}\overline{v'\theta'}$) from transient eddies (green lines; Fig. 2g) has the opposite sign to lower-level baroclinicity (green lines; Fig. 2g), indicating a negative rather than positive feedback. By contrast, the anomalous thermal forcing from quasi-stationary eddies (green lines; Fig. 2h) has the same sign as lower-level baroclinicity, indicating a positive feedback. This contrasting role of transient and quasi-stationary eddies in modulating lower-level baroclinicity under the jet core has been widely documented and arises from their different locations relative to the jet core [9, 17, 19, 20]. This baroclinic feedback is particularly strong during negative summer NAO extremes because Greenland blocking, the dominant component of quasi-stationary eddies in the Northern Hemisphere, is enhanced [4, 15]. This feedback is evident in Fig. 3b: the standardized linear slope between the lower-level high-latitude baroclinicity and the Greenland blocking index is much steeper during the decay stage (days +10 to +20; Fig. 3bii) than during the developing stage (days −5 to +5; Fig. 3bi) of negative summer NAO extremes. Its role in sustaining negative extremes is further supported by the decrease in this slope with time relative to onset (solid line; Fig. 3b).

2.3 Enhanced barotropic feedback increases positive extremes, and enhanced baroclinic feedback increases negative extremes

The primary goal of this study is to identify the mechanism driving the increased occurrence of both positive and negative phases of summer NAO extremes under global warming, as reported in a previous study [4]. Here, we show that MPI-GE-CMIP6 exhibits a similar increase (Fig. 4a) to that found in multiple models driven by CMIP5 forcing and reanalysis data [4]. Using the daily summer NAO index (Methods), we further show that this increase is primarily due to the enhanced persistence of summer NAO extremes (Fig. 4b). Combined with the previous section, these results suggest that the increase may be induced by enhanced eddy–mean-flow feedbacks under global warming.

Under global warming, the anticyclonic wave breaking that maintains positive summer NAO extremes is significantly enhanced (orange bars; Fig. 2a). This enhancement is consistent with the poleward strengthening of eddy momentum flux convergence (Fig. 5a) and EP-flux divergence (Fig. 5c), but it is not accompanied by stronger upward eddy transport, as indicated by mid-tropospheric eddy kinetic energy (Fig. 5e). Because the response is confined to anticyclonic wave breaking and eddy momentum flux convergence, rather than upward eddy transport, the increased persistence of positive summer NAO extremes is likely driven by stronger barotropic, rather than baroclinic, feedback. Indeed, the difference in zonal-mean flow after the onset of positive extremes (days 0–20) between the last and first 10 years of the simulation is predominantly barotropic (Fig. 5g). Such enhanced barotropic feedback is expected under global warming, as the critical latitude for Rossby wave breaking shifts poleward with the northward displacement of the background jet stream (Fig. S2b), consistent with the implications of Fig. 3a. Together, these results indicate that enhanced

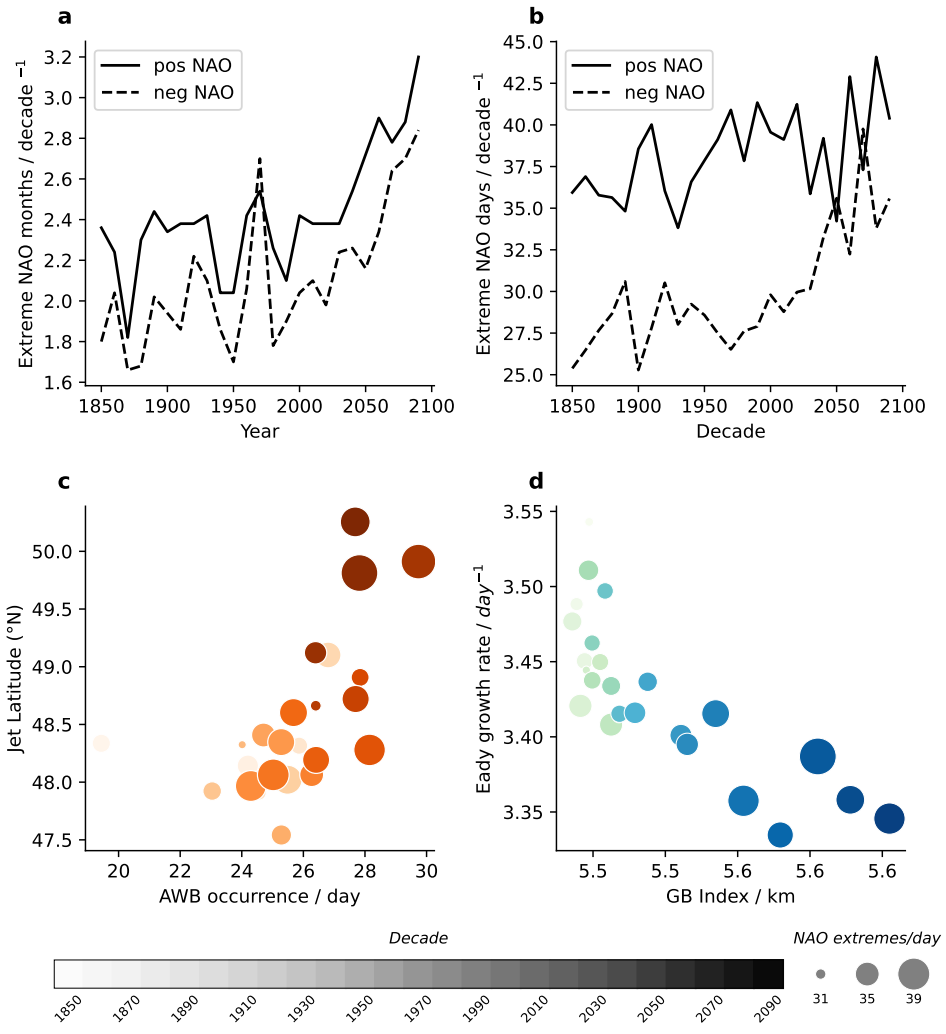

Fig. 4 Enhanced barotropic and baroclinic feedbacks increase positive and negative summer NAO extremes, respectively. a, Occurrence of summer NAO extremes identified from the monthly summer NAO index. **b**, Total number of days classified as summer NAO extremes based on the daily summer NAO index. **c**, Relationship between jet latitude and anticyclonic wave breaking for positive summer NAO extremes across decades. **d**, Relationship between the Eady growth rate and the Greenland blocking index for negative summer NAO extremes across decades. All composites are averaged over days 0–20 relative to the onset of summer NAO extremes to highlight the feedback stage. Anticyclonic wave breaking is shown as a decadal sum; all other quantities are shown as averages.

barotropic feedback associated with the northward shift of the jet stream increases positive summer NAO extremes, as shown in Fig. 4c.

The cyclonic wave breaking also increases with global warming (green bars; Fig. 2b), but this is unlikely the primary mechanism driving the increase in negative summer NAO extremes, because the cyclonic wave breaking is not the dominant contributor to their persistence. Instead, the enhanced EP-flux divergence that prolongs negative extremes in a warmer climate (green bars; Fig. 2; Fig. 5d) is driven by enhanced baroclinic feedback. This enhancement is evident from the significant increase in mid-tropospheric eddy kinetic energy (green bars; Fig. 2f; Fig. 5f), the stronger lower-level baroclinicity (green bars; Fig. 2e), and the enhanced thermal forcing from quasi-stationary eddies (green bars; Fig. 2h) at the later stage of negative summer NAO extremes. Furthermore, the difference in zonal-mean flow after the onset of negative extremes between the last and the first 10 years of simulations is predominantly baroclinic (Fig. 5h), in contrast to that of positive extremes (Fig. 5g). This stronger baroclinic feedback is consistent with the increased variability of eddy thermal forcing from quasi-stationary eddies under global warming (Fig. S2d). Therefore, enhanced baroclinic feedback associated with stronger high-latitude blocking increases negative summer NAO extremes, as shown in Fig. 4d.

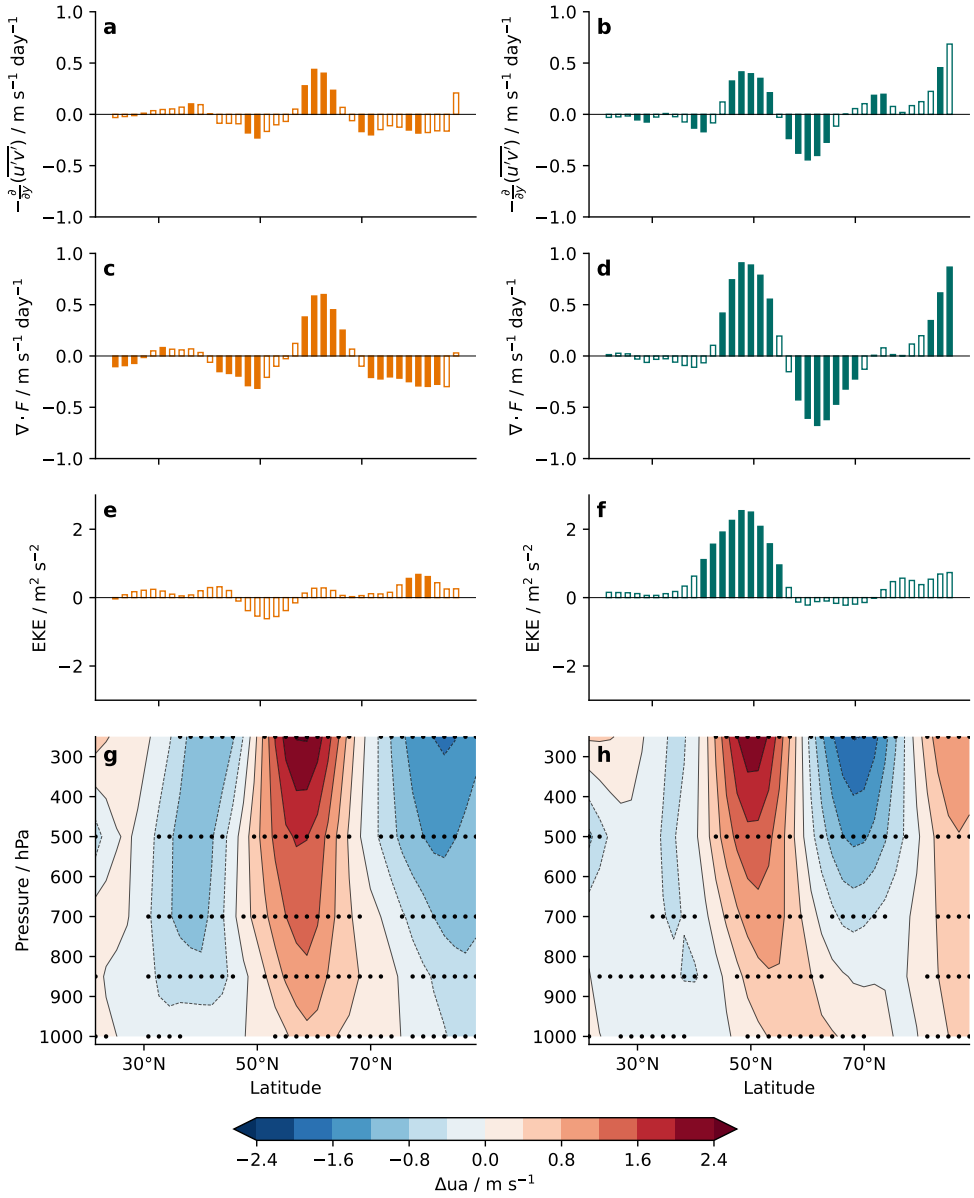

Fig. 5 Both barotropic and baroclinic feedbacks strengthen under global warming. Panels show changes in composites between the last and first 10 years of the simulations for eddy momentum flux convergence (**a,b**), EP-flux convergence (**c,d**), mid-latitude eddy kinetic energy (**e,f**), and zonal-mean flow (**g,h**). The first column shows composites for positive summer NAO extremes, and the second column shows composites for negative summer NAO extremes. All composites are averaged over days 0–20 relative to the onset of the extremes to highlight the feedback stage. Eddy momentum flux convergence and EP-flux convergence are shown at 250 hPa, and eddy kinetic energy is shown at 500 hPa. All quantities are zonally averaged over 90°W–40°E. Filled bars and dotted shadings indicate statistical significance at the 95% confidence level.

3 Conclusion and discussion

Using daliy output from MPI-GE-CMIP6, we identify enhanced eddy–mean-flow feedbacks as the underlying physical mechansim driving more summer NAO extremes under global warming. To do so, we first show that eddy forcing of U anomalies and Rossby wave breaking drive the occurrence of summer NAO extremes. We then show that barotropic and baroclinic feedbacks sustain positive and negative summer NAO extremes, respectively. Finally, we show that both feedbacks strengthen under global warming: barotropic feedback strengthens due to northward-shifted jet stream, and baroclinic feedback strengthen due to enhanced atmospheric blocking.

Our study suggests that the "tug-of-war" between a strengthened jet stream [21–23], driven by an increased upper-level meridional temperature gradient [21, 24, 25], and enhanced blocking [26, 27], potentially driven by Arctic amplification [28], only represents changes in the mean-state of the atmospheric flow. These two responses, however, have their corresponding effects on the positive and negative phases of summer NAO extremes, leading to a higher probability of contrasting extreme weather between northern Europe and the Mediterranean under global warming.

4 Data and Method

4.1 Data

This study uses the Max Planck Institute for Meteorology Grand Ensemble forced with historical and Shared Socioeconomic Pathway 5–8.5 (SSP5-8.5) CMIP6 forcing (MPI-GE-CMIP6) [14]. We use monthly and daily output to identify summer NAO extremes and daily output to calculate momentum flux and heat flux carried by atmospheric eddies. The analysis focuses on the extended boreal summer (May–September).

4.2 Summer NAO extremes

We decompose the NAO pattern using empirical orthogonal function (EOF) analysis of monthly 500-hPa geopotential height along ensemble dimension, following [4]. We then compute monthly and daily summer NAO indices by projecting detrended geopotential height anomalies onto this pattern. We define summer NAO extremes as cases in which the NAO index exceeds ± 1.5 standard deviations. For daily extremes, we additionally require event persistence of more than 5 days, with a one-day tolerance. In total, we obtain over 9000 positive extremes and over 8000 negative extremes across all decades and ensemble members.

4.3 Rossby wave breaking

Rossby wave-breaking events are identified as overturning of the dynamical tropopause on isentropes (2 PVU contours; 1 PVU $\equiv 1 \times 10^{-6}\,\mathrm{K\,kg^{-1}\,m^2\,s^{-1}}$) [29]. We first calculate potential temperature and potential vorticity (PV) on pressure levels, then interpolate the PV field to isentropic levels from 295 to 360 K at 5 K intervals, following [29]. We then apply a wave-breaking detection algorithm [30] to all isentropes. Detected events are classified as anticyclonic wave breaking (AWB) when the magnitude (defined as the field-mean transient eddy momentum flux; Following [31]) is positive, and as cyclonic wave breaking when it is negative. The identified events vary across isentropic levels and the occurrence increase at higher isentropes under global warming (Fig. S4). To increase robustness, all plots show the summed occurrence of these events across isentropic levels.

4.4 The transient eddies and the quasi-stationary eddies

We define transient eddies as the high-frequency component of the flow with periods of 2–12 days (Fig. S3a), following [31]. In practice, transient-eddy terms (e.g., u', v', θ') are obtained by applying a 2–12-day band-pass filter to daily fields.

We define quasi-stationary eddies as zonal anomalies of the low-frequency flow (Fig. S3b), following [32]. In practice, quasi-stationary-eddy terms are obtained by first applying a 30-day running mean to daily fields and then subtracting the ensemble-mean zonal mean of the filtered field.

4.5 EP-flux divergence

To account for water-vapor effects transported by eddies, we use equivalent potential temperature instead of potential temperature when calculating eddy heat flux, following the moist Eliassen–Palm (EP) flux formulation [33, 34].

4.6 Lower-level baroclinicity

Baroclinicity is approximated by the Eady growth rate [35], defined as:

$$\sigma_E \approx 0.31 \cdot \frac{f}{N} \left| \frac{\partial \mathbf{v}}{\partial z} \right| \tag{4}$$

where σ_E is the Eady growth rate, f is the Coriolis parameter, N is the Brunt–Väisälä frequency, defined as $N = \sqrt{\frac{g}{\theta}\frac{\partial \theta}{\partial z}}$, where g is gravitational acceleration and θ is the potential temperature, $\frac{\partial \mathbf{v}}{\partial z}$ is the vertical shear of the wind, z is the vertical height, $\mathbf{v}$ is the horizontal wind. In this study, since we focus on the effects of the zonal mean of the eddy thermal forcing, only the vertical shear of the zonal wind ($\frac{\partial u}{\partial z}$) is used in the calculation. The low-level baroclinicity is represented as the Eady growth rate at 850 hPa.

4.7 Wavenumber-Phase speed spectra analysis

We apply wavenumber–phase-speed spectral analysis to the eddy terms along all Northern Hemisphere latitude circles, following [36]. We then sum contributions across

all wavenumbers to obtain the latitude–phase-speed distribution, or across all phase speeds to obtain the latitude–wavenumber distribution of eddy variance.

5 Supplementary Information

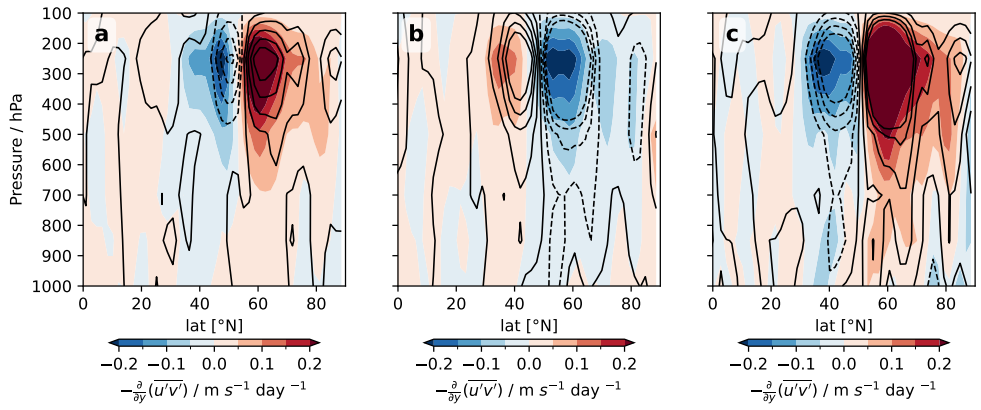

Fig. S1 Anomalous eddy momentum forcing by transient eddies drives the meridional shift of the upper-level zonal-mean flow. a, Zonal mean of the composite-mean anomalous eddy momentum forcing ($-\frac{\partial}{\partial y}\overline{u'v'}$) for positive summer NAO extremes. **b**, Same as **a**, but for negative summer NAO extremes. **c**, Difference between **a** and **b**. Composites are averaged over days $[-10, 5]$ relative to the onset of the summer NAO extremes. Shadings show the first 10 years (1850–1859), and contours show the last 10 years (2090–2099).

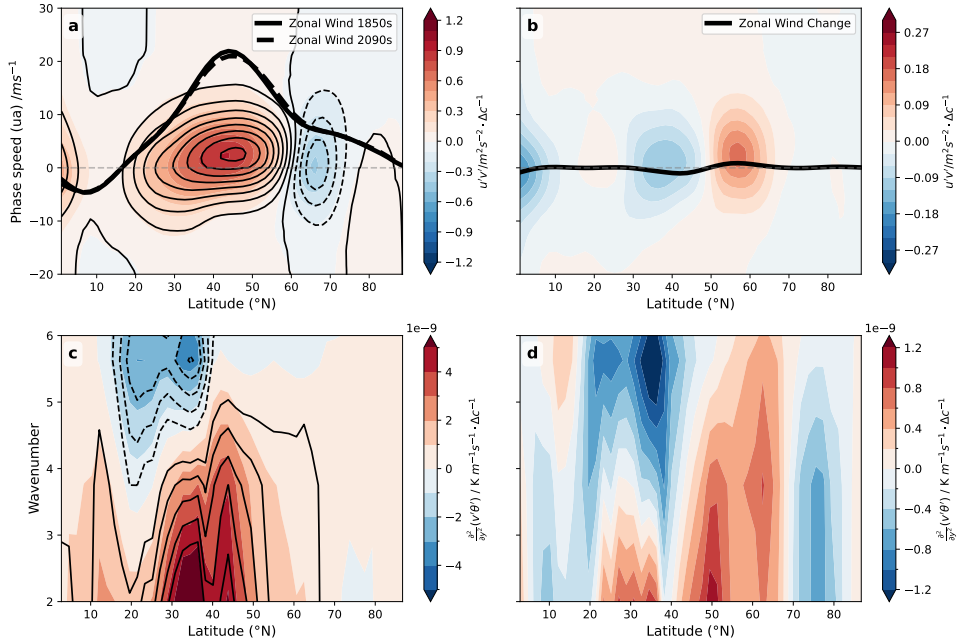

Fig. S2 As in Fig. 2, but without removing the climatology. Panels show composites of EP-flux convergence (**a**), Eady growth rate (**b**) and eddy kinetic energy (**c,d**). Quantities in **a-c** are averaged over the northern flank of the jet [−90°, 40°, 50°, 70°]. Panel **d** shows the eddy kinetic energy averaged over the jet core [−90°, 40°, 40°, 70°].

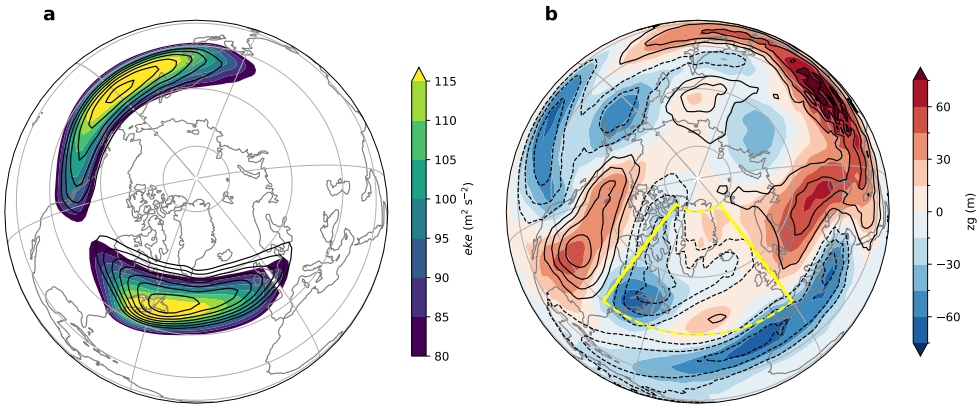

Fig. S3 Transient eddies and quasi-stationary eddies over the Northern Hemisphere in summer. a, The climatology of the eddy kinetic energy of the transient eddies at 250 hPa. Shadings for 1850s (pre-industrial-like climate) and contours for 2090s (4K warmer climate). **b**, Quasi-stationary eddies in high latitudes at 250 hPa.Shadings for 1850s and contours for 2090s.

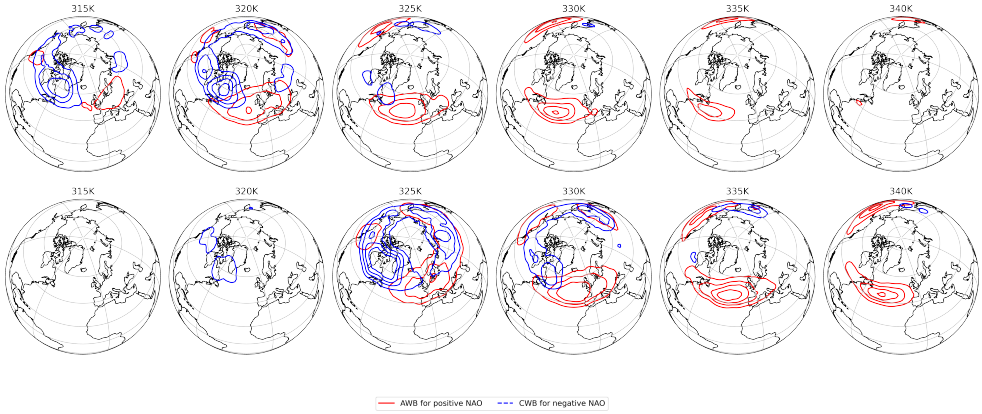

Fig. S4 Rossby wave breaking associated with summer NAO extremes. a–f, Rossby wave breaking during summer NAO extremes in the 1850s. Contours for cyclonic wave breaking (blue) range from 2 to 10, with an interval of 2. Contours for anticyclonic wave breaking (red) range from 4 to 20, with an interval of 4. Labels at the top of each panel indicate isentropic levels. **g–l**, Same as **a–f**, but for the 2090s.

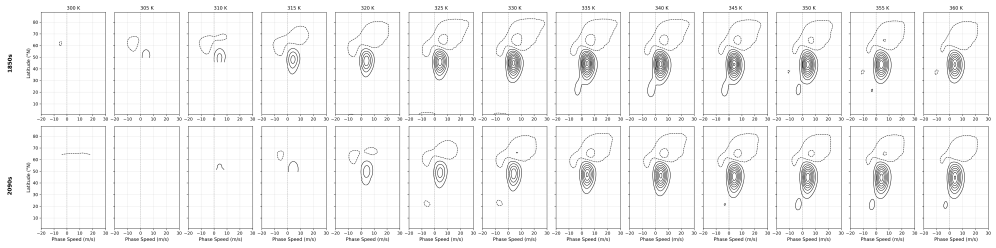

Fig. S5 Rossby wave propagation at different isentropes. a-f, Co-spectra of transient eddy momentum flux as a function of latitude and phase speed during 1850s. **g-l**, Same as **a-f**, but for 2090s. Contours range from -1.21 to 1.21, with an interval of 0.1. Units $m^2 s^{-1} \cdot c^{-1}$.

References

[1] Saravanan, R. Atmospheric low-frequency variability and its relationship to mid-latitude sst variability: Studies using the ncar climate system model. *Journal of Climate* **11**, 1386–1404 (1998).

[2] Hurrell, J. W. Decadal trends in the North Atlantic Oscillation: Regional temperatures and precipitation. *Science* **269**, 676–679 (1995).

[3] Walker, G. & Bliss, E. Memoirs of the royal meteorological society. *World weather V* **4**, 53–84 (1932).

[4] Liu, Q., Bader, J., Jungclaus, J. H. & Matei, D. More extreme summertime north atlantic oscillation under climate change. *Communications Earth & Environment* **6**, 1–12 (2025).

[5] Vallis, G. K., Gerber, E. P., Kushner, P. J. & Cash, B. A. A mechanism and simple dynamical model of the north atlantic oscillation and annular modes. *Journal of the atmospheric sciences* **61**, 264–280 (2004).

[6] Gerber, E. P. & Vallis, G. K. On the zonal structure of the north atlantic oscillation and annular modes. *Journal of the Atmospheric Sciences* **66**, 332–352 (2009).

[7] Vallis, G. K. *Atmospheric and oceanic fluid dynamics* (Cambridge University Press, 2017).

[8] Edmon Jr, H., Hoskins, B. & McIntyre, M. Eliassen-palm cross sections for the troposphere. *Journal of Atmospheric Sciences* **37**, 2600–2616 (1980).

[9] Zhang, Y., Yang, X.-Q., Nie, Y. & Chen, G. Annular mode–like variation in a multilayer quasigeostrophic model. *Journal of the Atmospheric Sciences* **69**,

2940–2958 (2012).

[10] Lorenz, D. J. A simple mechanistic model of wave–mean flow feedbacks, poleward jet shifts, and the annular mode. *Journal of the Atmospheric Sciences* **80**, 549–568 (2023).

[11] Robinson, W. A. A baroclinic mechanism for the eddy feedback on the zonal index. *Journal of the Atmospheric Sciences* **57**, 415–422 (2000).

[12] Lorenz, D. J. The role of barotropic versus baroclinic feedbacks on the eddy response to annular mode zonal wind anomalies. *Journal of the Atmospheric Sciences* **79**, 2529–2547 (2022).

[13] Lorenz, D. J. & Hartmann, D. L. Eddy–zonal flow feedback in the southern hemisphere. *Journal of the atmospheric sciences* **58**, 3312–3327 (2001).

[14] Olonscheck, D. *et al.* The new max planck institute grand ensemble with cmip6 forcing and high-frequency model output. *Journal of Advances in Modeling Earth Systems* **15**, e2023MS003790 (2023).

[15] Woollings, T., Hannachi, A., Hoskins, B. & Turner, A. A regime view of the North Atlantic Oscillation and its response to anthropogenic forcing. *Journal of Climate* **23**, 1291–1307 (2010).

[16] Eliassen, A. On the transfer of energy in stationary mountain waves. *Geofys. Publ.* **22**, 1–23 (1961).

[17] Nie, Y., Zhang, Y., Yang, X.-Q. & Chen, G. Baroclinic anomalies associated with the southern hemisphere annular mode: Roles of synoptic and low-frequency eddies. *Geophysical Research Letters* **40**, 2361–2366 (2013).

[18] James, I. N. & James, I. N. *Introduction to circulating atmospheres* (Cambridge University Press, 1995).

[19] Gerber, E. P. & Vallis, G. K. Eddy–zonal flow interactions and the persistence of the zonal index. *Journal of the Atmospheric Sciences* **64**, 3296–3311 (2007).

[20] Inatsu, M., Mukougawa, H. & Xie, S.-P. Atmospheric response to zonal variations in midlatitude sst: Transient and stationary eddies and their feedback. *Journal of climate* **16**, 3314–3329 (2003).

[21] Shaw, T. A. & Miyawaki, O. Fast upper-level jet stream winds get faster under climate change. *Nature Climate Change* **14**, 61–67 (2024).

[22] Woollings, T., Drouard, M., O'Reilly, C. H., Sexton, D. M. & McSweeney, C. Trends in the atmospheric jet streams are emerging in observations and could be linked to tropical warming. *Communications Earth & Environment* **4**, 125 (2023).

[23] Ossó, A. *et al.* Advancing our understanding of eddy-driven jet stream responses to climate change–a roadmap. *Current Climate Change Reports* **11**, 2 (2024).

[24] Lee, S. H., Williams, P. D. & Frame, T. H. Increased shear in the North Atlantic upper-level jet stream over the past four decades. *Nature* **572**, 639–642 (2019).

[25] Lorenz, D. J. & DeWeaver, E. T. Tropopause height and zonal wind response to global warming in the IPCC scenario integrations. *Journal of Geophysical Research: Atmospheres* **112** (2007).

[26] Coumou, D., Lehmann, J. & Beckmann, J. The weakening summer circulation in the Northern Hemisphere mid-latitudes. *Science* **348**, 324–327 (2015).

[27] Shaw, T. A., Miyawaki, O., Chou, H.-H. & Blackport, R. Fast-get-faster explains wavier upper-level jet stream under climate change. *Communications Earth & Environment* **5**, 653 (2024).

[28] Preece, J. R. *et al.* Summer atmospheric circulation over greenland in response to arctic amplification and diminished spring snow cover. *Nature Communications* **14**, 3759 (2023).

[29] Wernli, H. & Sprenger, M. Identification and era-15 climatology of potential vorticity streamers and cutoffs near the extratropical tropopause. *Journal of the atmospheric sciences* **64**, 1569–1586 (2007).

[30] Kaderli, S. skaderli/wavebreaking: Wavebreaking v0.3.8. Zenodo (2024). Version 0.3.8.

[31] Rivière, G. & Orlanski, I. Characteristics of the atlantic storm-track eddy activity and its relation with the north atlantic oscillation. *Journal of the Atmospheric Sciences* **64**, 241–266 (2007).

[32] Limpasuvan, V. & Hartmann, D. L. Wave-maintained annular modes of climate variability. *Journal of Climate* **13**, 4414–4429 (2000).

[33] Dwyer, J. G. & O'Gorman, P. A. Moist formulations of the eliassen–palm flux and their connection to the surface westerlies. *Journal of the Atmospheric Sciences* **74**, 513–530 (2017).

[34] Yamada, R. & Pauluis, O. Momentum balance and eliassen–palm flux on moist isentropic surfaces. *Journal of the Atmospheric Sciences* **73**, 1293–1314 (2016).

[35] Hoskins, B. J. & Valdes, P. J. On the existence of storm-tracks. *Journal of Atmospheric Sciences* **47**, 1854–1864 (1990).

[36] RANDEL, W. & HELD, I. Phase speed spectra of transient eddy fluxes and critical layer absorption. *Journal of the atmospheric sciences* **48**, 688–697 (1991).